Electronic Supplementary Material (ESI) for New Journal of Chemistry.
This journal is © The Royal Society of Chemistry and the Centre National de la Recherche Scientifique 2017

# Bi(III) immobilization inside MIL-101: enhanced photocatalytic performance

Konstantin A. Kovalenko,[a,b*] Natalia V. Ruban,[b] Sergey A. Adonin,[a,b] Denis V. Korneev,[c] Simon B. Erenburg,[a,d] Svetlana V. Trubina,[a] Kristina Kvashnina,[e,f] Maxim N. Sokolov,[a,g] and Vladimir P. Fedin[a,b]

[a] Nikolaev Institute of Inorganic Chemistry SB RAS, 3 Lavrentiev Av., 630090 Novosibirsk, Russia

[b] Novosibirsk State University, 2 Pirogova St., 630090 Novosibirsk, Russia

[c] State Research Centre for Virology and Biotechnology “Vector”, 630559 Koltsovo, Novosibirsk Region, Russia

[d] Budker Institute of Nuclear Physics SB RAS, 11 Lavrentiev Av., 630090 Novosibirsk, Russia

[e] European Synchrotron Radiation Facility, BP 220, 38043, Grenoble Cedex, France, EU

[f] Helmholtz-Zentrum Dresden-Rossendorf (HZDR), Institute of Resource Ecology – P.O. Box 510119, 01314, Dresden, Germany, EU

[g] Kazan Federal University, Alexander Butlerov Institute of Chemistry, Lobachevskogo str. 1/29, 420008, Kazan, Russia

# Supporting Information

## Contents:

## 1. MIL-101 structure

MIL-101 has a zeolite-like structure with micropores 8 Å and two types of mesopores (30 and 38 Å) (Figure S1).

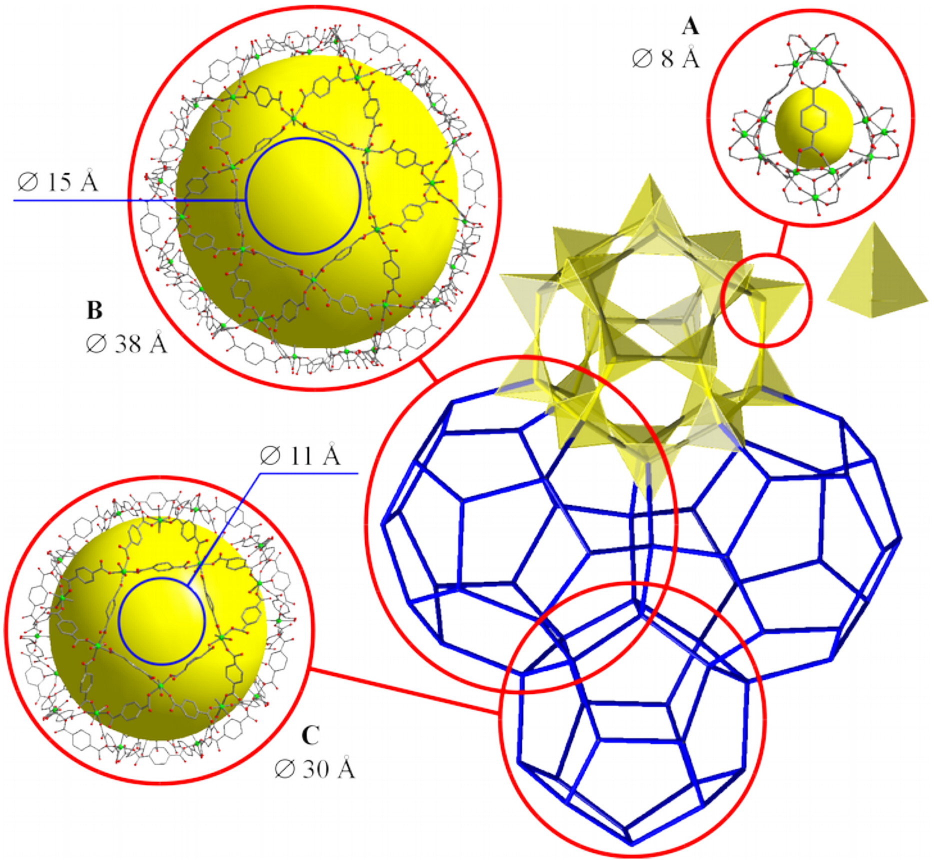

**Figure S1.** A schematic representation of the MIL-101 porous structure. Metal clusters $\{Cr_3O(O_2CR)_6\}$ are linked by terephthalate ions in tetrahedral building units (**A**), which form a zeolite-type framework with two types of mesopores: large (**B**) and small (**C**). Yellow spheres represent the available volume inside the building units, blue circles — the windows between the neighboring cavities.

## 2. Characterisation of compounds

### 2.1. Element analysis

The chemical analysis of solid samples was carried out using X-Ray fluorescence spectroscopy in several nanoscale points for control of samples uniformity. The data are summarized in Table S1.

**Table S1.** Elemental analysis data of Bi(III)@MIL-101 before and after catalysis.

**Bi(III)@MIL-101 (1)**

| Point | wt. % | | | atomic ratio | | Bi per f.u.[1] | Cl per f.u. | Bi per mesocage |
|---|---|---|---|---|---|---|---|---|
| | **Cl** | **Cr** | **Bi** | **Cr/Bi** | **Cl/Bi** | | | |
| 1 | 11.41 | 78.96 | 9.63 | 32.967 | 6.985 | 0.091 | 0.636 | 1.03 |
| 2 | 12.80 | 77.82 | 9.38 | 33.333 | 8.043 | 0.090 | 0.724 | 1.02 |
| 3 | 14.50 | 76.67 | 8.83 | 34.884 | 9.681 | 0.086 | 0.833 | 0.97 |
| 4 | 10.28 | 79.78 | 9.94 | 32.258 | 6.097 | 0.093 | 0.567 | 1.05 |
| **Average** | **12.25** | **78.31** | **9.45** | **33.361** | **7.701** | **0.090** | **0.690** | **1.02** |
| $\sigma_n$ | 1.82 | 1.36 | 0.47 | 1.109 | 1.541 | 0.003 | 0.115 | 0.03 |

**Bi(III)@MIL-101 after 4 catalytic cycles**

| Point | wt. % | | | atomic ratio | | Bi per f.u. | Cl per f.u. | Bi per mesocage |
|---|---|---|---|---|---|---|---|---|
| | **Cl** | **Cr** | **Bi** | **Cr/Bi** | **Cl/Bi** | | | |
| 1 | 11.73 | 78.59 | 9.68 | 32.609 | 7.141 | 0.092 | 0.657 | 1.04 |
| 2 | 12.81 | 78.37 | 8.82 | 35.714 | 8.560 | 0.084 | 0.719 | 0.95 |
| 3 | 12.21 | 78.44 | 9.35 | 33.708 | 7.697 | 0.089 | 0.685 | 1.01 |
| **Average** | **12.25** | **78.47** | **9.29** | **34.010** | **7.799** | **0.088** | **0.687** | **1.00** |
| $\sigma_n$ | 0.54 | 0.11 | 0.44 | 1.575 | 0.715 | 0.004 | 0.031 | 0.05 |

[1] formula unit of MIL-101 is $[Cr_3O(bdc)_3]X$ (bdc — terephthalate anion $C_6H_4(COO)_2^{2-}$, X — counteranion: $F^-$, $NO_3^-$, $OH^-$, $Cl^-$).

According to the element analysis, the Cr/Bi/Cl ratio in Bi(III)@MIL-101 (**1**) is 1:0.030:0.231 = 3:0.09:0.69. The unit cell of MIL-101 contain 816 Cr atoms, 16 smaller cavities and 8 larger cavities. According to this fact the Bi content is 3·0.030 = 0.09 per formula unit of MIL-101 $[Cr_3O(bdc)_3F(H_2O)_2]$ or 816·0.030/24 ≈ 1.02 per mesocage (both types of cavities with smaller and larger size). The chloride amount is *ca.* 8 times bigger than bismuth amount. But it should be noted that chloride anions have two functions inside matrix: 1) forming BiOCl particles; 2) neutralization of framework charge. The MIL-101 framework with formula unit $[Cr_3O(bdc)_3]^+$ has positive charge which is compensated in the initial MIL-101 compound by the fluoride or nitrate. After treatment by solution with very high chloride content ($BiCl_3$ solution in 2 M HCl) the fluoride and nitrate have been partially substituted by chloride. The driving force of this process is possibility for the chloride to penetrate into tetrahedral microcages of the framework which was clearly demonstrated in our recent paper [2]. The amount of chloride is in a good agreement with number of such microcages. There are 816 Cr atoms in the unit cell, that is 272 $\{Cr_3O(O_2CR)_6\}$ clusters. The supertetrahedra each are composed of four clusters. Taking into account that every cluster belongs to two adjacent tetrahedra (Fig. S1), their total amount is of 136 per unit cell or 0.5 per formula unit. Therefore each tetrahedral microcage is occupied by one chloride anion what is in a good agreement with previous result [2]. In the other hand the chloride content is less than needed for charge neutralization what is meant that fluoride or nitrate are also remain inside matrix.

## 2.2. Powder X-Ray diffraction

Here we presented additional PXRD patterns not included in the main text as well as patterns in more broad range.

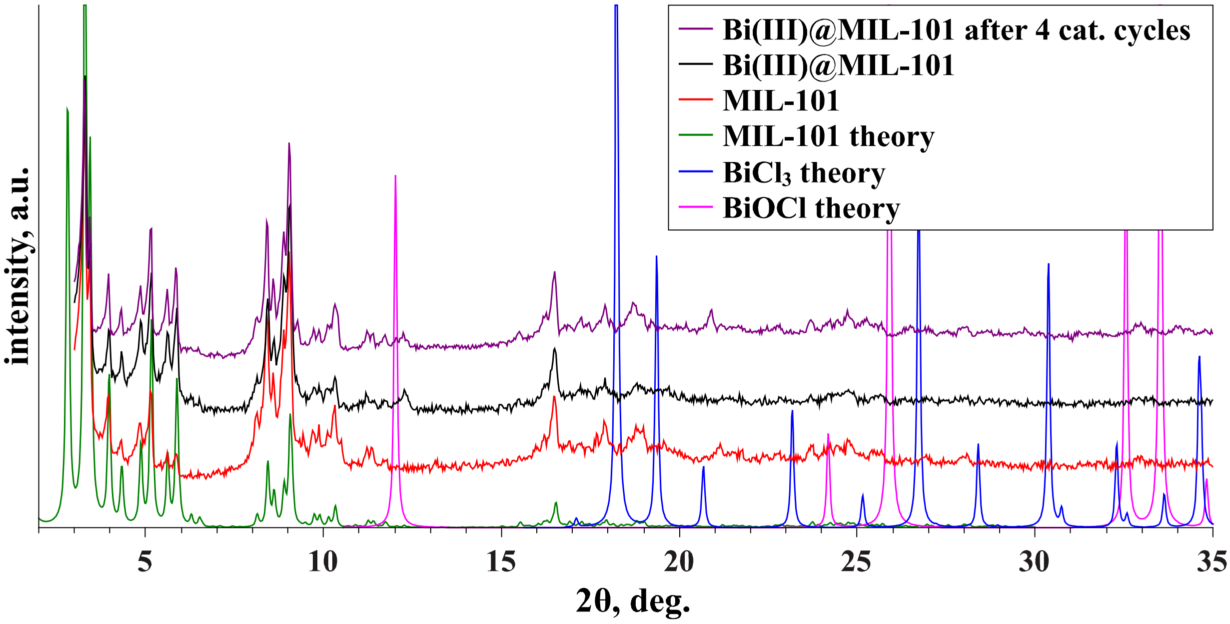

**Figure S2.** PXRD patterns for Cr-MIL-101 (red), Bi(III)@MIL-101 before (black) and after (purple) catalytic tests. Theoretical patterns for MIL-101 (green), $BiCl_3$ (blue) and BiOCl (pink) are given for comparison.

## 2.3. EXAFS-HERFD

High-energy-resolution X-ray absorption measurements were performed at the beamline ID26 of the European Synchrotron Radiation Facility. The electrons energy was 6.0 GeV, the ring electron current varied between 180 and 200 mA. The energy of X-ray incident beam was selected using the reflection from a double Si[111] crystal monochromator. Rejection of higher harmonics was achieved by two Si mirrors with a Pd and Cr layers located at 2.5 mrad angle relative to the incident beam. The energy calibration was performed using a Bi metal sample. High-energy-resolution fluorescence detection (HERFD) spectra were measured with an X-ray emission spectrometer at 12 K. The Bi HERFD spectra at the $L_3$-edge were obtained by recording the intensity of the Bi $L_{\alpha 1}$ emission line (10839 eV) as a function of the incident energy. The emission energy was selected using the <660> reflection of four spherically bent Ge crystal analyzers (with $R$ = 1 m). Each Bi HERFD-XANES scan was collected in 30 s with a step size of 0.1 eV and usually used averaging of 10–20 scans (see Fig. S3). Full Bi EXAFS-HERFD spectra over a 1000 eV range were measured in 180 s with a step size of 0.2 eV and averaging of 5 scans.

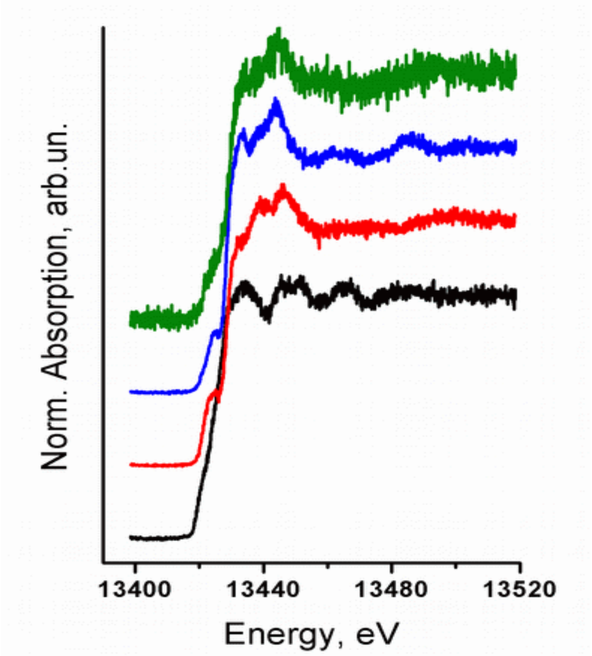

**Figure S3.** Bi$L_3$ HERFD XANES spectra of: BiOCl – blue; Bi(III)@MIL-101 – green and Bi$L_3$ HERFD XANES reference spectra: Bi metal – black; $Bi_2O_3$ – red.

Cl*K* HERFD XANES spectra of samples obtained in similar synthetic condition without and with presence of mesoporous metal-organic matrix MIL-101 (BiOCl and Bi(III)@MIL-101) are shown on Fig. S4.

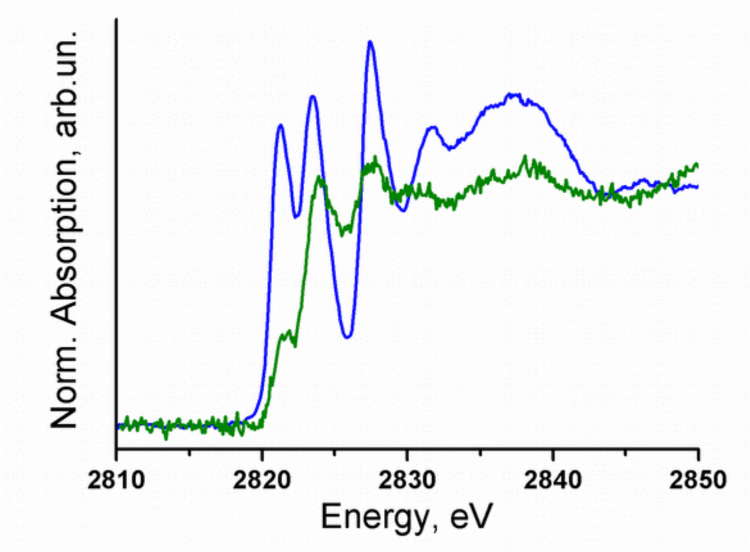

**Figure S4.** Cl*K* HERFD XANES spectra of the samples: BiOCl — blue; Bi(III)@MIL-101 – green.

Samples for measurement XAS spectra were compressed into tablets with cellulose as filler.

The preprocessing of the absorption spectra was performed using the VIPER program [3]. The local environment of Bi atoms were simulated for data filtered by the Fourier method ($\Delta R$ = 1.2–4.1 Å) with $k^2$ weighing ($k^2\chi(k)$ Bi$L_3$) within the wave vector range of 3–11 Å$^{-1}$ ($T$ = 12 K) and using the EXCURV 98 program [4]. In data processing the phase and amplitude characteristics were calculated in the von Bart and Hedin approximation. The amplitude suppression $S_0^2$ due to multielectron processes was determined for a Bi metal and then the obtained value ($S_0^2$ = 0.8) was set and fixed during simulation spectra of studied samples. Fig. S5 shows good agreement between experimental and model EXAFS spectra. The local structure parameters (the interatomic distances

(*R*), partial coordination numbers (*N*), Debye–Waller factors ($2\sigma^2$) were determined in the simulation process (“fitting”) of EXAFS data. (see Table S2).

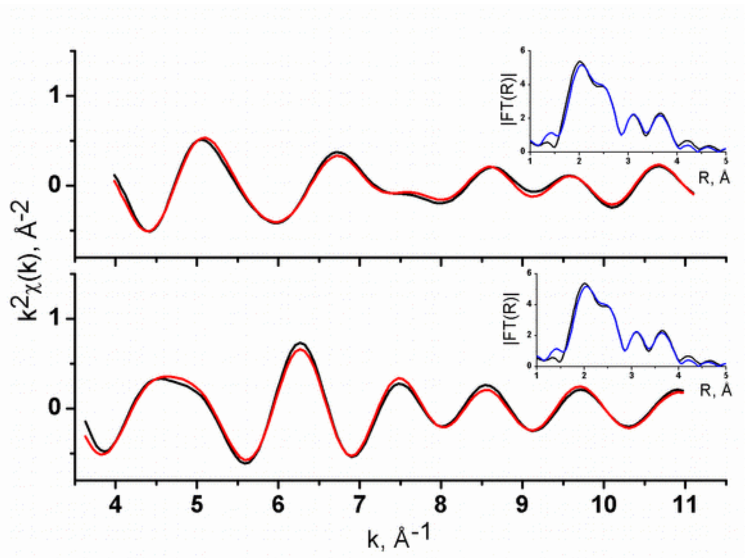

**Figure S5.** Comparison of experimental (black line) EXAFS spectra ($k^2\chi(k)$), Fourier filtered in $\Delta R$ = 1.2 – 3.6 Å, with simulated (model) spectra (red line) for samples BiOCl (lower row) and Bi(III)@MIL-101 (upper row). The enclosed figures show radial distribution functions (black lines – experimental functions, blue lines — model).

**Table S2.** Parameters of samples microstructure, obtained by the simulation process from the EXAFS spectra. N – partial coordination numbers, R – interatomic distances, $2\sigma^2$ – Debye-Waller factor.

| Sample | Absorbing atom–Backscattering atom | *N* | *R*, Å | $2\sigma^2$, Å$^2$ |
|---|---|---|---|---|
| BiOCl | Bi – O | 1.6±0.3 | 2.18±0.01 | 0.003±0.001 |
| | Bi – Cl | 1.8±0.3 | 2.48±0.02 | 0.003±0.001 |
| | Bi – Bi | 2.6±0.5 | 2.52±0.02 | 0.009±0.002 |
| | Bi – O | 2.4±0.3 | 3.26±0.04 | 0.003±0.001 |
| | Bi – Cl | 1.5±0.4 | 3.34±0.03 | 0.003±0.001 |
| | Bi – Cl | 0.5±0.1 | 3.52±0.04 | 0.003±0.001 |
| Bi(III)@MIL-101 | Bi – O | 1.2±0.2 | 2.05±0.01 | 0.003±0.001 |
| | Bi – O | 1.9±0.3 | 2.53±0.02 | 0.003±0.001 |
| | Bi – O | 2.1±0.4 | 2.67±0.02 | 0.009±0.002 |
| | Bi – O | 1.1±0.3 | 2.88±0.03 | 0.003±0.001 |
| | Bi – Bi | 2.0±0.3 | 3.24±0.02 | 0.003±0.001 |

## 2.4. Bismuth-oxygen coordination types according to Cambridge crystallographic database

**Table S3.** Bismuth-oxygen coordination types according to Cambridge crystallographic database

| Coordination type | | Hits in CSDB | Mean distance, Å |
|---|---|---|---|
| A | $\text{Bi–OH}_2$ | 118 | 2.597±0.035 |
| B | Bi–OH | 87 | 2.464±0.050 |
| C | $\text{Bi}\overset{(1)}{–}\text{OH}_2\overset{(2)}{–}\text{Bi}$ | 3 | (1) 2.718±0.014<br>(2) 2.801±0.013 |
| D | $\text{Bi}\overset{(1)}{–}\text{OH}\overset{(2)}{–}\text{Bi}$ | 25 | (1) 2.358±0.036<br>(2) 2.361±0.026 |

|  |  |  |  |
|---|---|---|---|
| E | (1) (2)<br>Bi–O–Bi | 283 | (1) 2.301±0.058<br>(2) 2.408±0.069 |
| F | (1) (2)<br>Bi–OH–Bi<br>\|(3)<br>Bi | 13 | (1) 2.333±0.013<br>(2) 2.341±0.021<br>(3) 2.374±0.043 |
| G | (1) (2)<br>Bi–O–Bi<br>\|(3)<br>Bi | 68 | (1) 2.209±0.033<br>(2) 2.309±0.049<br>(3) 2.453±0.074 |
| H | 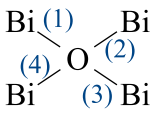 | 26 | (1) 2.195±0.031<br>(2) 2.333±0.046<br>(3) 2.465±0.062<br>(4) 2.606±0.090 |

Comparison of X-Ray structural data for layered BiOCl (according to []) and EXAFS data obtained was performed. The coordination number of bismuth in layered BiOCl is 8, four bonds are Bi–O with mean distance 2.31 Å and other four bonds are Bi–Cl with mean distance 3.06 Å. The same coordination numbers and distances are observed according to EXAFS data (Table S2): the number of Bi–O bonds are 4 with mean distance 2.83 Å, while the number of Bi–Cl bonds are 3.8 with mean distance 2.96 Å.

### 2.5. Nitrogen sorption

The ratio of the micro and mesopores significantly changes after treatment with $BiCl_3$/HCl solution and following treatment by ammonia solution: in the latter case the percentage of the micropores decreases. The treatment with chloride containing solution and the appearance of the chloride anions in the Cr-MIL-101 structure most likely affects the distribution of guest molecules inside the porous frameworks and partially blocks the access to the supertetrahedra with respect to gaseous adsorbates, e.g. nitrogen employed in this analysis. In our previous paper [2] it was shown that chlorides occupy microcages inside supertetrahedra. Therefore, the maxima corresponding to microcages on differential curve of the pore size distribution are decreased.

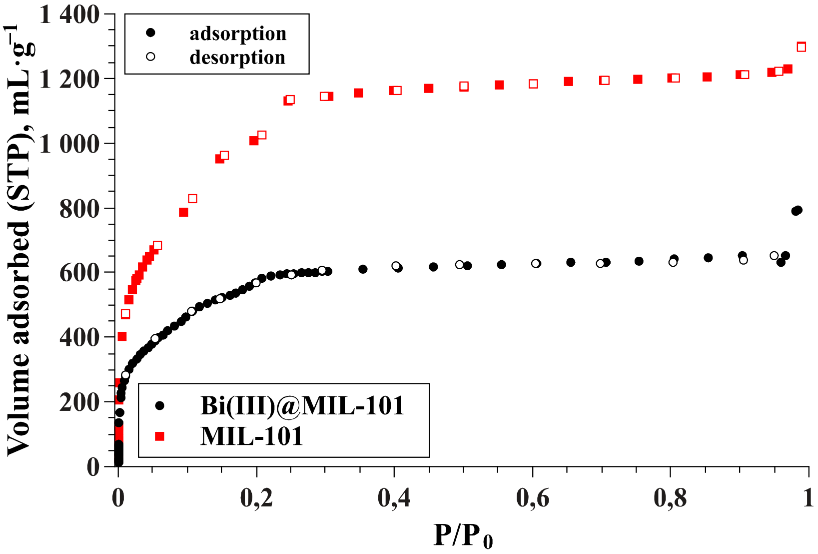

**Figure S6.** Nitrogen sorption isotherms at 77 K on MIL-101 and Bi(III)@MIL-101.

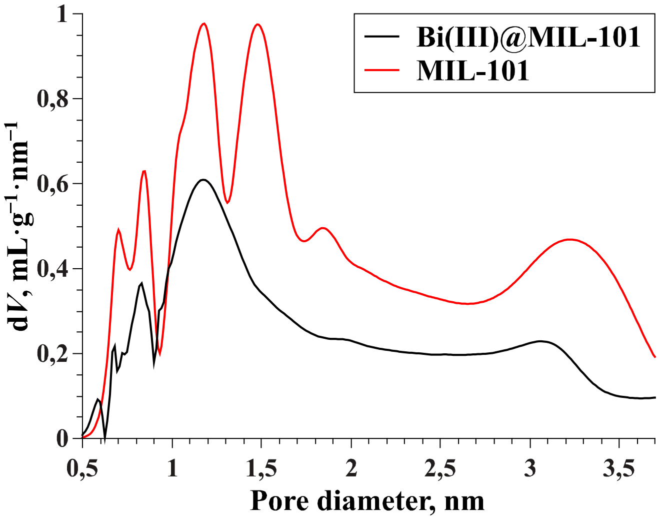

**Figure S7.** Saito&Foley pore size distribution in Bi(III)@MIL-101 (black) and MIL-101 (red).

## 2.6. TEM Examination

The crystals of MIL-101 and Bi(III)@MIL-101 were examined by TEM (JEM 1400, Jeol, Japan, 120 kV) with standard sample preparation. The BiOCl nanoparticles are not visible in the TEM images of Bi(III)@MIL-101 after the first impregnation (Fig. 8). The crystals have size about 200 nm and the same shape as pristine MIL-101. However, twice and triple impregnated samples significantly differ from the once impregnated sample: there are a lot of bulky particles on the MIL-101 crystal's surface (See Fig. 1 in main text).

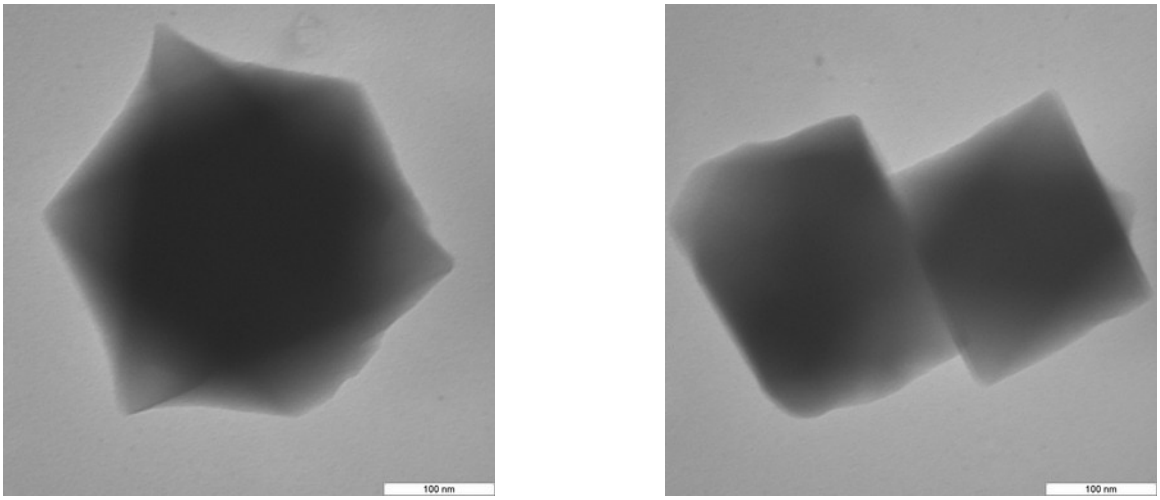

**Figure S8.** TEM images of Bi(III)@MIL-101.

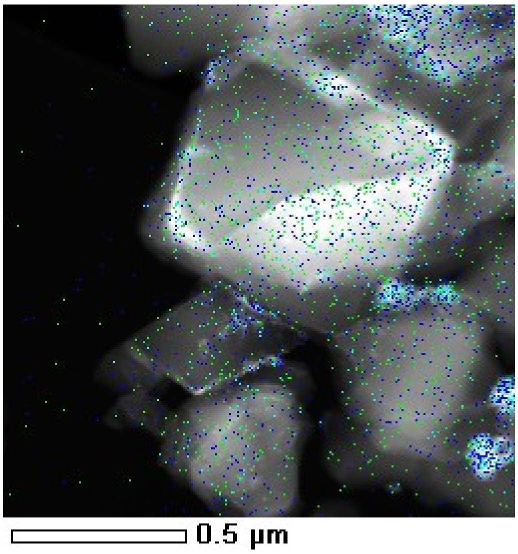

**Figure S9.** EDS mapping of Bi(III)@MIL-101 crystals: Cr — green dots, Bi — dark-blue dots.

# 3. Catalytic Tests

## 3.1. Comparison of MIL-101, Bi(III)@MIL-101 and layred BiOCl

**Table S3.** Photocatalytic degradation of methyl red.

| **Time of irradiation, min** | **Dye, %** | | |
|---|---|---|---|
| | **MIL-101, 15 mg** | **Bi(III)@MIL-101, 15 mg** | **BiOCl, 10 mg** |
| 0 | 100 | 100 | 100 |
| 10 | 99 | 65 | 20 |
| 20 | 99 | 48 | 1 |
| 30 | 100 | 24 | — |
| 40 | 99 | 9 | — |

## 3.2. Description of “portionwise addition” experiment

1) The catalyst (15 mg of Bi(III)@MIL-101, containing *ca.* 0.4 mg of Bi, or 10 mg of pure BiOCl, containing *ca.* 8 mg of Bi) was added to a solution of methyl red (10 mL, $3.5\cdot10^{-5}$ M or 10 mg·L$^{-1}$) containing 200 μL of 1 M HCl for pH adjusting.

2) The mixture was irradiated by Hg lamp during 10 min after that the Vis spectrum was recorded and concentrating of methyl red founded.

3) The 2nd stage was repeated 5–6 times (when using Bi(III)@MIL-101) or 2 times (when using pure BiOCl as catalyst) until full decolorizing of solution (according to Vis spectrum) not observed. So the full experimental time of irradiating in one cycle is 60 minutes for Bi(III)@MIL-101 or 20 minutes for pure BiOCl.

4) After full decolorizing the small portion of concentrated solution of methyl red was added (200 μL, $1.82\cdot10^{-3}$ M) to recover the initial concentration of the dye.

5) The stages 2 and 3 have been repeated at least 4 times.

### 3.3. Pure BiOCl Comparison Experiment. *m*(BiOCl) = 10 mg

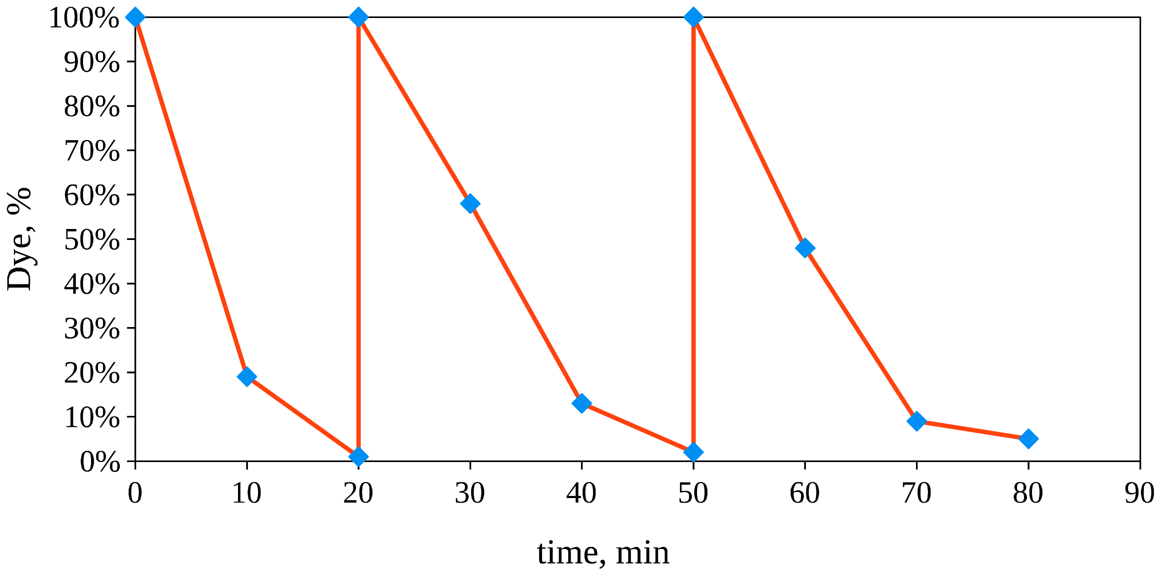

**Figure S10.** Pure BiOCl photocatalytic performance in several catalytic cycles.

## 4. References

[1] Férey, G.; Mellot-Draznieks, C.; Serre, C.; Millange, F.; Dutour, J.; Surblé, S.; Margiolak, I. *Science*, **2005**, *309*, 2040-2042.

[2] Berdonosova, E. A.; Kovalenko, K. A. *et. al. J. Phys. Chem. C*, **2015**, *119* (23), 13098–13104. DOI: 10.1021/acs.jpcc.5b02861

[3] Klementiev, K.V. *J. Phys. D: Appl. Phys.* **2001**, *34*, 209.

[4] Binsted, N. EXCURV98:CCLRC Daresbury Laboratory Computer Program (**1998**).